

CHAOS IN UNDERWATER ACOUSTICS

MICHAEL G. BROWN, FREDERICK D. TAPPERT,
GUSTAVO J. GONI, AND KEVIN B. SMITH

Rosenstiel School of Marine and Atmospheric Science
University of Miami, 4600 Rickenbacker Cswy.
Miami, FL 33149

ABSTRACT. The range-dependent sound propagation problem differs in a fundamental way from the range-independent problem, at least in the geometric limit. In the range-independent problem the divergence between neighboring ray trajectories is slow (power law behavior). In the generic range-dependent problem some ray trajectories exhibit extreme sensitivity to initial conditions (chaotic behavior) wherein neighboring trajectories diverge exponentially. Using simple range-dependent models of oceanic waveguides, involving both volume and boundary structure, the chaotic behavior of sound rays is discussed and illustrated via the construction of Poincare sections, the calculation of power spectra, and the calculation of Lyapunov exponents. It is argued that under chaotic conditions ray trajectories are not computable beyond some finite predictability horizon. Under conditions in which ray trajectories are predominantly chaotic, the growth in range of the complexity of the wavefield is shown to be exponential: the number of eigenrays connecting a fixed source and receiver grows exponentially while the average intensity of ray arrivals decays exponentially. Some preliminary attempts to investigate the extent to which the chaotic behavior of ray trajectories carries over to finite frequency wavefields are discussed.

1. INTRODUCTION

When it is assumed that the ocean's sound speed varies as a function of depth only and the ocean boundaries coincide with surfaces of constant depth, then the acoustic wave equation can be solved by a variety of techniques which depend on separating variables. This assumption is frequently unjustified. The solution to the range-dependent problem differs in a fundamental way from the solution to the range-independent problem, at least in the geometric limit. In the range-dependent problem there is no Snell invariant, and ray trajectories may exhibit chaotic motion, i.e., extreme sensitivity to initial conditions. This extreme sensitivity to initial conditions leads to a limited ability to predict acoustic fields.

In the following sections these ideas are illustrated by examining

sound ray propagation in two simple range-dependent oceanic waveguides. In the first, the ocean boundaries are flat but the sound speed in the ocean volume depends on both depth and range. The second waveguide consists of a range-independent downward refracting ocean volume overlying a bottom with range-dependent bathymetric variations. The latter problem is examined by introducing an area-preserving mapping to replace the ray equations. Both problems are discussed and analyzed in the context of recent developments in the studies of integrable and nonintegrable Hamiltonian systems. Our emphasis on Hamiltonian dynamics is natural inasmuch as the acoustic ray equations have Hamiltonian form.

Detailed modern discussions of Hamiltonian systems can be found in Henon (1983) and Lichtenberg and Lieberman (1982). Our presentation is largely pedagogical, in the hope that readers who are not familiar with these topics will be able to follow the presentation. We state without proof many results which are discussed in the aforementioned references. The novelty of our work is the application of these results to the underwater sound propagation problem. Results of similar studies have been presented by Palmer et al. (1988) and Abdullaev and Zaslavskii (1988).

2. RAY CHAOS IN THE OCEAN VOLUME

The ray equations consistent with the parabolic wave equation are (see Tappert, 1977)

$$\frac{dz}{dr} = \frac{\partial H}{\partial p}, \quad \frac{dp}{dr} = -\frac{\partial H}{\partial z}, \quad (1a,b)$$

where

$$H(z,p,r) = \frac{1}{2} p^2 + V(z,r). \quad (1c)$$

Here z and r are depth and range, respectively, and, by equations (1), $p = dz/dr = \tan \theta$ where θ is the ray angle with respect to the horizontal.

The potential $V(z,r)$ may be thought of as either $\frac{1}{2} (1 - c_0^2/c^2(z,r))$ or $c(z,r)/c_0 - 1$ where $c(z,r)$ is the sound speed and c_0 is a reference value.

These equations define a Hamiltonian system with one degree of freedom. Note that range is the time-like variable in these equations. If $V = V(z)$ (range-independent problem), the system is said to be autonomous. If $V = V(z,r)$ (range-dependent problem) the system is said to be nonautonomous. This distinction is crucial. It is most easily understood by examining the geometry of ray trajectories.

2.1 Ray Geometry

Solutions to equations (1) are trajectories $z(r)$, $p(r)$, which lie in the three-dimensional space (z,p,r) . We shall confine our attention to the special case of sound speed structures which are periodic in r , $c(z,r) = c(z,r + \lambda)$. Then r can be defined modulo λ without loss of generality. Although this case is special, it suffices to illustrate all of the important ideas. Additionally, in the oceanic waveguides considered here, both ray depth and ray angle are bounded. With these assumptions ray trajectories

lie in the bounded three dimensional space (z,p,r) . There are two fundamentally different types of trajectory - those which fill volumes in (z,p,r) and those which lie on two-dimensional surfaces in this three dimensional space.

All trajectories are of the latter type (termed "regular") if the system is integrable, i.e., if there exists a constant of the motion $I(z,p,r)$ for which

$$\frac{dI}{dr} = \frac{\partial I}{\partial z} \frac{dz}{dr} + \frac{\partial I}{\partial p} \frac{dp}{dr} + \frac{\partial I}{\partial r} = 0. \quad (2)$$

If such a function exists each trajectory lies on a surface of constant I , thereby reducing the dimension of the accessible space from three to two. In a bounded phase space these surfaces are tori. Thus, in an integrable system with a bounded phase space, ray trajectories lie on a set of nested tori.

This is the situation encountered in a range-independent environment. Here $H(z,p)$ is a constant of the motion - the first two terms on the rhs of (2) cancel by (1) and the third term is zero. In range-dependent environments it is extremely rare that there exists a constant of the motion: generically, in range-dependent environments, the acoustic ray equations are nonintegrable. Before discussing this situation further we introduce a simple technique - first used by Poincare - which is now commonly used to distinguish between area and volume filling trajectories. To distinguish between the two cases one need only examine a two-dimensional slice of the three-dimensional space. On this slice, volume and area filling trajectories in (z,p,r) will fill areas and lie on smooth curves, respectively.

For the periodically range dependent problems considered here, the simplest way to construct such a Poincare section is to view the ray trajectories, $z(r)$, $p(r)$, stroboscopically at integer multiples of λ , $z(n\lambda)$, $p(n\lambda)$, $n = 0,1,2,\dots$. Some examples are shown in figure 1. Here, the trajectories, $z(r)$, $p(r)$, were numerically computed for many sets of initial conditions, $z(0)$, $p(0)$, using a perturbed Munk (1974) potential,

$$V(z,r) = \epsilon(e^{-\eta} + \eta - 1) + \delta \frac{2z}{B} e^{-2z/B} \cos(2\pi/\lambda). \quad (3)$$

Here $\eta = 2(z - z_a)/B$ is a scaled depth coordinate, $z_a = 1$ km is the sound channel axis depth, the depth scale $B = 1$ km, and $\epsilon = 0.0057$. In figure 1 the wavelength of the range dependent perturbation λ was taken to be 10 km while the perturbation strength δ was varied.

The first plot in figure 1 corresponds to the range-independent case, $\delta = 0$. Here, for each set of initial conditions, the succession of points plotted all lie on smooth curves. (In some cases the curves appear to be broken because so few (500) points are plotted.) This is expected because in this case the ray equations are integrable. As the strength of the range-dependent perturbation δ increases, some of these closed curves break up into a series of closed curves ("islands") surrounded by speckled regions ("chaotic seas"). This phenomenon is due to a resonance between unperturbed ($\delta = 0$) rays and the range dependent perturbation. The rays which form the five island structure, for instance, have a wavelength very close to 50 km. The 10 km wavelength perturbation induces a 5:1

ident oceanic waveguides. sound speed in the ocean second waveguide consists ocean volume overlying a ns. The latter problem is pping to replace the ray ralyzed in the context of rable and nonintegrable nian dynamics is natural ltonian form.

systems can be found in 82). Our presentation is ho are not familiar with ation. We state without aforementioned references. of these results to the s of similar studies have Abdullaev and Zaslavskii

c wave equation are (see

(1a,b)

(1c)

and, by equations (1), $p =$ respect to the horizontal. her $\frac{1}{2} (1 - c_0^2/c^2(z,r))$ or id c_0 is a reference value. ith one degree of freedom. e equations. If $V = V(z)$ to be autonomous. If V system is said to be is most easily understood

), $p(r)$, which lie in the fine our attention to the periodic in r , $c(z,r) = c(z,r)$ without loss of generality. strate all of the important considered here, both ray assumptions ray trajectories

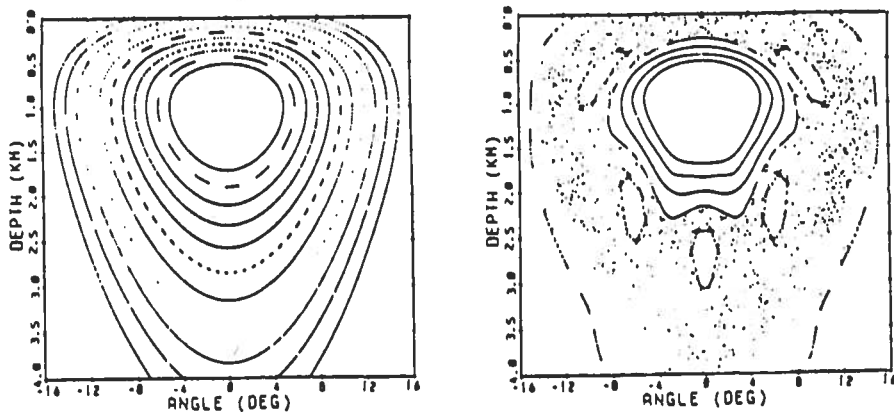


Figure 1. Poincaré sections computed using the potential $V(z,r)$ given in equation (3). In both cases the initial ray depth $z_0 = 1$ km and the initial ray angles are $\theta_0 = 5^\circ, 6^\circ, \dots, 15^\circ$. 500 points are plotted for each ray trajectory. Left: $\delta = 0$. Right: $\delta = 0.01$.

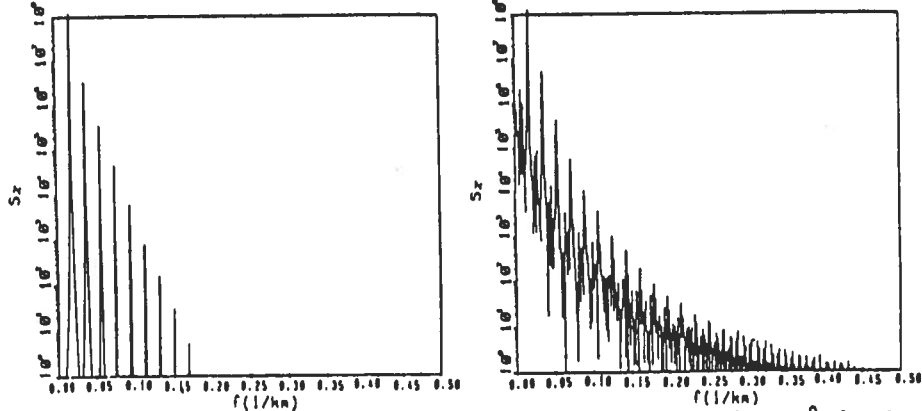


Figure 2. Power spectra of two ray trajectories $z(r)$. Left: $z_0 = 1$ km, $\theta_0 = 11^\circ$, $\delta = 0$. Right: $z_0 = 1$ km, $\theta_0 = 12^\circ$, $\delta = 0.01$.

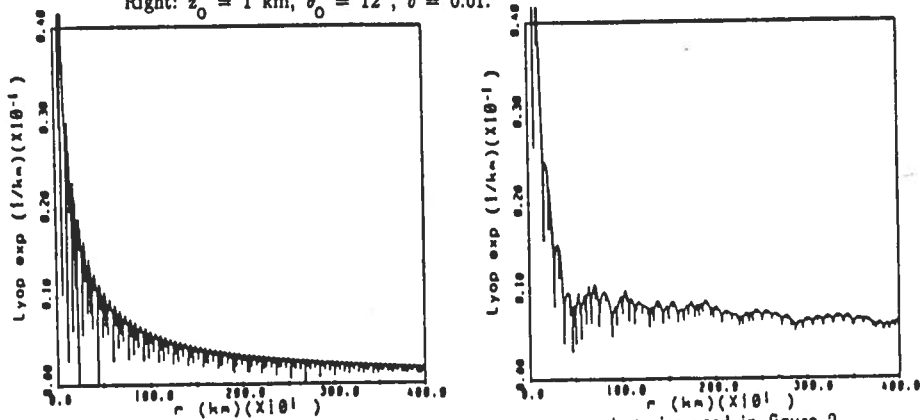


Figure 3. Plots of $(1/r)$ in $|\lambda_1(r)|$ vs. r for the same two trajectories used in figure 2.

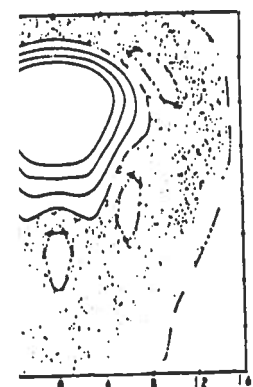
resonance and 5 islands are formed. The ray trajectories which form the speckled regions surrounding the islands (not seen in all cases) are termed "chaotic". They correspond to volume filling (in (z,p,r)) rays. A further increase in the strength of the range-dependent perturbation causes the regular barriers (termed "KAM invariant tori" for reasons discussed below) separating neighboring chaotic seas to break down, thereby forming larger connected chaotic regions.

All of this behavior is typical of integrable bounded Hamiltonian systems which are subjected to a nonintegrable perturbation. A central result to understanding this problem is the Kolmogorov-Arnol'd-Moser (KAM) theorem which states that when an integrable Hamiltonian system (range-independent sound speed structure) is subjected to a nonintegrable (range-dependent) perturbation, regular motion is preserved for most trajectories. Stated somewhat differently, the KAM theorem guarantees that most of the regular tori associated with an integrable Hamiltonian system survive a small perturbation to the Hamiltonian, although the tori become slightly distorted. When coupled with numerical simulations of the type shown in figure 1, this theorem provides important insight into the behavior of acoustic ray trajectories in weakly range-dependent oceans.

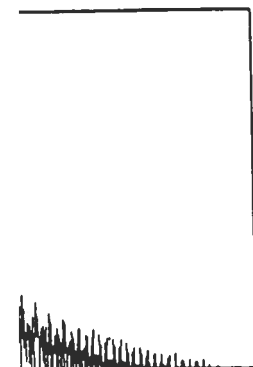
The Poincare sections shown in this figure give some geometric insight into the difference between regular and chaotic (a precise definition will be given later) ray trajectories. An important observation is that regular trajectories, because each such trajectory is constrained to lie on one of a set of smooth embedded surfaces, diverge from each other only very slowly. Chaotic trajectories, on the other hand, form a tangled web in phase space, becoming hopelessly intertwined with many other trajectories, possibly with very different initial conditions. Under such conditions the motion of individual ray trajectories cannot be predicted at long range and neighboring trajectories diverge very rapidly. These ideas will be discussed in more detail below.

2.2 Power Spectra

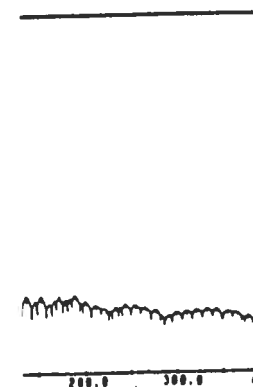
Power spectra of $z(r)$ provide additional insight into the difference between regular and chaotic trajectories. Spectra of regular trajectories consist of a finite number of isolated lines while spectra of chaotic trajectories are continuous and appear to be noisy. The connection between regular motion and discrete spectra can be seen geometrically. Motion on a torus is most naturally described using action-angle variables. In these coordinates the motion is periodic. Because the transformation between action-angle variable and $z(r)$, $p(r)$ is generally nonlinear, harmonics will be present in spectra of the latter. These spectra remain discrete, however. The connection between regular trajectories and discrete spectra can also be rationalized by noting that the long time evolution of such systems are predictable: all that is required is a knowledge of the wavenumbers, amplitudes, and phases of a finite number of sinusoids. The long time evolution of a chaotic system is, on the other hand, effectively unpredictable. This is consistent with a continuous, noisy spectrum. These ideas are illustrated in figure 2. Here, power spectra of $z(r)$ for two rays are shown. The first case corresponds to $\delta = 0$, the range-independent problem. Here, all trajectories are regular. The power spectrum of the



GLE (DEG)
 in equation (3). In
 are $\theta_0 = 5^\circ, 6^\circ, \dots, 15^\circ$
 $\delta = 0.01$.



$f(1/km)$
 1 km, $\theta_0 = 11^\circ$, $\delta = 0$.



$(km)(\times 10^1)$
 rays used in figure 2.

trajectory shown consists of a small number of lines, as expected. The second spectrum was computed using one of the rays which fills the large chaotic sea in the $\delta = 0.01$ calculation shown in figure 1. The spectrum of this chaotic trajectory is broad band and noisy.

2.3 Lyapunov Exponents

We have seen that Poincare sections and power spectra are useful for addressing the question of whether a ray trajectory is chaotic. The Lyapunov exponent provides more information - it is a measure of how chaotic a trajectory is. The most important feature that distinguishes chaotic and regular motion is that under chaotic conditions neighboring ray trajectories diverge exponentially while under regular conditions the divergence is governed by a power law. The Lyapunov exponent is a quantitative measure of this divergence. After describing how Lyapunov exponents are calculated, we consider some of the implications of chaotic motion.

The variational equations follow from the ray equations (1) upon setting $\xi = \delta z$, $\eta = \delta p$,

$$\frac{d}{dr} \begin{bmatrix} \xi \\ \eta \end{bmatrix} = \begin{bmatrix} \frac{\partial^2 H}{\partial p \partial z} & \frac{\partial^2 H}{\partial p^2} \\ -\frac{\partial^2 H}{\partial z^2} & -\frac{\partial^2 H}{\partial z \partial p} \end{bmatrix} \begin{bmatrix} \xi \\ \eta \end{bmatrix} = \begin{bmatrix} 0 & 1 \\ -\frac{\partial^2 V}{\partial z^2} & 0 \end{bmatrix} \begin{bmatrix} \xi \\ \eta \end{bmatrix} \quad (4)$$

These equations describe how small elements $\delta z \delta p$ of phase space are stretched along a ray trajectory. The variational equations (4) and the ray equations (1) define a system of four coupled equations which can be integrated to give $z(r)$, $p(r)$, $\xi(r)$, and $\eta(r)$ given a knowledge of their initial conditions $z(0)$, $p(0)$, $\xi(0)$, and $\eta(0)$. The variational equations can be combined to give

$$\frac{d^2 \xi}{dr^2} + \left[\frac{\partial^2 V}{\partial z^2} \right] \xi = 0. \quad (5)$$

Assume that $\xi_1(r)$ and $\xi_2(r)$, with

$$\xi_1(0) = 1, \quad \frac{d\xi_1}{dr}(0) = 0, \quad (6a)$$

$$\xi_2(0) = 0, \quad \frac{d\xi_2}{dr}(0) = 1, \quad (6b)$$

are two solutions to (5). They are linearly independent as their Wronskian is unity,

$$W(r) = W(0) = \xi_1(0) \frac{d\xi_2}{dr}(0) - \xi_2(0) \frac{d\xi_1}{dr}(0) = 1. \quad (7)$$

(The Wronskian is constant because the coefficient of $d\xi/dr$ in (5) is zero.) Note that from the first of the variational equations (4) $d\xi/dr = \eta$. It then follows from (7) that the Jacobi matrix

lines, as expected. The rays which fills the large figure 1. The spectrum

$$J(r) = \begin{bmatrix} \xi_1(r) & \xi_2(r) \\ \eta_1(r) & \eta_2(r) \end{bmatrix} \quad (8)$$

has determinant 1. The Jacobi matrix allows us to study sensitivity to initial conditions,

$$\begin{bmatrix} dz(r) \\ dp(r) \end{bmatrix} = \begin{bmatrix} \frac{\partial z}{\partial z_0}(r) & \frac{\partial z}{\partial p_0}(r) \\ \frac{\partial p}{\partial z_0}(r) & \frac{\partial p}{\partial p_0}(r) \end{bmatrix} \begin{bmatrix} dz_0 \\ dp_0 \end{bmatrix} = J(r) \begin{bmatrix} dz_0 \\ dp_0 \end{bmatrix} \quad (9)$$

Let $\lambda_i(r)$ and $\bar{u}_i(r)$, $i = 1, 2$, with $|\lambda_1(r)| \geq |\lambda_2(r)|$, denote the eigenvalues and eigenvectors of $J(r)$. Because $\det J(r) = 1$, $\lambda_1(r) \lambda_2(r) = 1$. The solution to (9), $[dz \ dp]^T$, is a linear combination of $\lambda_i(r) \bar{u}_i(r)$. Under chaotic conditions

$$|\lambda_1(r)| \sim e^{\nu r} \text{ and } |\lambda_2(r)| \sim e^{-\nu r} \text{ as } r \rightarrow \infty. \quad (10)$$

The Lyapunov exponent is defined as

$$\nu \equiv \lim_{r \rightarrow \infty} \frac{1}{r} \ln |\lambda_1(r)|. \quad (11)$$

For a regular trajectory (10) is replaced by power law growth and decay of $\lambda_1(r)$ and $\lambda_2(r)$, respectively, and ν defined in (11) is zero.

Plots of $(1/r) \ln |\lambda_1(r)|$ vs r are shown in figure 3 for the same two trajectories that were used to produce figure 2. For the regular trajectory this curve appears to be approaching $\nu = 0$, while for the chaotic trajectory the curve appears to be approaching a value of ν close to $(200 \text{ km})^{-1}$. This behavior is consistent with the results shown in both figures 1 and 2.

We now consider one of the implications of exponential sensitivity to initial conditions associated with chaotic ray motion. Suppose we attempt to find the eigenrays connecting a fixed source and receiver separated by a distance r . This might be done by computing the trajectories of many rays, each leaving the source with a different angle θ , out to range r . If the ray depth at range r lies within some specified tolerance of the receiver depth we say that we have found an eigenray. Suppose we find by trial and error that in order to meet this tolerance criterion at range r , the ray launch angle must be specified with n_r bits of precision. It is natural to ask how n_r varies as a function of r . Under chaotic conditions n_r is proportional to r . The proportionality constant is the (scaled) Lyapunov exponent. If, for instance, θ must be specified with 12 bits of precision at $r = 120 \text{ km}$ and $\nu (= \nu/\ln 2)$ is $(10 \text{ km})^{-1}$, then each 10 km increase in range would require another bit of precision in the specification of the launch angle. In this example 20 bits would be required to find eigenrays

er spectra are useful for
ectory is chaotic. The
it is a measure of how
feature that distinguishes
conditions neighboring ray
regular conditons the
Lyapunov exponent is a
describing how Lyapunov
he implications of chaotic

ray equations (1) upon

$$\begin{bmatrix} 0 & 1 \\ -\frac{\partial^2 V}{\partial z^2} & 0 \end{bmatrix} \begin{bmatrix} \xi \\ \eta \end{bmatrix} \quad (4)$$

$\delta z \delta p$ of phase space are
equations (4) and the ray
equations which can be
ven a knowledge of their
variational equations can

(5)

(6a)

(6b)

endent as their Wronskian

$$\frac{d\xi_1}{dr}(0) = 1. \quad (7)$$

it of $d\xi/dr$ in (5) is zero.)
tions (4) $d\xi/dr = \eta$. It

at $r = 200$ km, 30 bits would be required at 300 km, etc. One quickly runs into limitations imposed by finite precision computers. On a machine in which floating point numbers are stored with a 24 bit mantissa, eigenrays could be found only out to a range of somewhat less than 240 km in our example. At longer ranges, attempts to iteratively search for eigenrays are doomed to failure. Computed ray trajectories at these longer ranges will have effectively forgotten their initial conditions. With these ideas in mind, it is natural to refer to ν^{-1} as a "predictability horizon", an order of magnitude estimate of the range over which a ray trajectory can be predicted.

These ideas also provide some insight into a commonly given definition of chaos: chaos is unpredictable behavior in a low order dynamical system associated with extreme sensitivity to initial conditions.

3. RAY CHAOS INDUCED BY BOUNDARY INTERACTIONS

We now turn our attention to sound ray propagation in a simple ocean model in which ray trajectories interact with a range dependent boundary. The techniques used to study this problem differ somewhat from those used earlier. Here, the ray dynamics are studied using an area preserving mapping.

3.1 An Area Preserving Mapping

We consider sound ray propagation in a topless ocean in which the sound speed increases with height above the bottom so that rays are downward refracted. We assume that the bottom bathymetry $z_b(r)$ is known and that the bottom is rigid so that rays are specularly reflected. Let r_n and θ_n be the range and angle (in radians) at which a ray intersects the bottom. The situation is shown schematically in figure 4. If $z_b(r)$ is small compared to the turning height of a ray, then the bottom displacement can be neglected when determining the intersection of the ray with the bottom. This approximation allows the ray dynamics to be studied using the mapping

$$\theta_{n+1} = \theta_n + 2z'_b(r_n), \quad (12a)$$

$$r_{n+1} = r_n + B(\theta_{n+1}). \quad (12b)$$

Here $z'_b(r)$ is the bottom slope and $B(\theta)$ is the increment in range of the ray that leaves (and returns to) the bottom with angle θ . Equation (12a) says that upon reflection the outgoing ray angle is equal to the incoming ray angle plus twice the local bottom slope. Equation (12b) incrementally updates the total range traversed by a ray.

We shall assume that

$$z_b(r) = -h \cos(kr) \quad (13)$$

and

c. One quickly
 On a machine
 4 bit mantissa,
 at less than 240
 tively search for
 at these longer
 ns. With these
 lity horizon", an
 y trajectory can
 commonly given
 n a low order
 ial conditions.

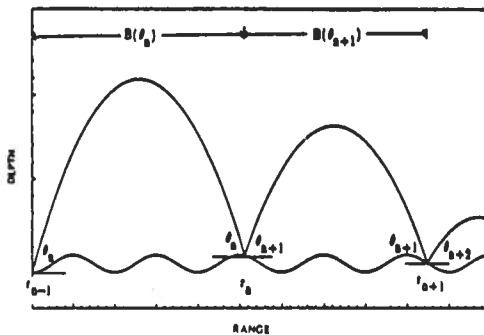


Figure 4. Segment of a ray in a downward refracting ocean overlying a sinusoidal bottom.

CTIONS

a simple ocean
 endent boundary.
 from those used
 area preserving

which the sound
 ys are downward
 (r) is known and
 cted. Let r_n and
 ray intersects the
 e 4. If $z_b(r)$ is
 then the bottom
 section of the ray
 dynamics to be

(12a)

(12b)

at in range of the
 9. Equation (12a)
 d to the incoming
 (12b) incrementally

(13)

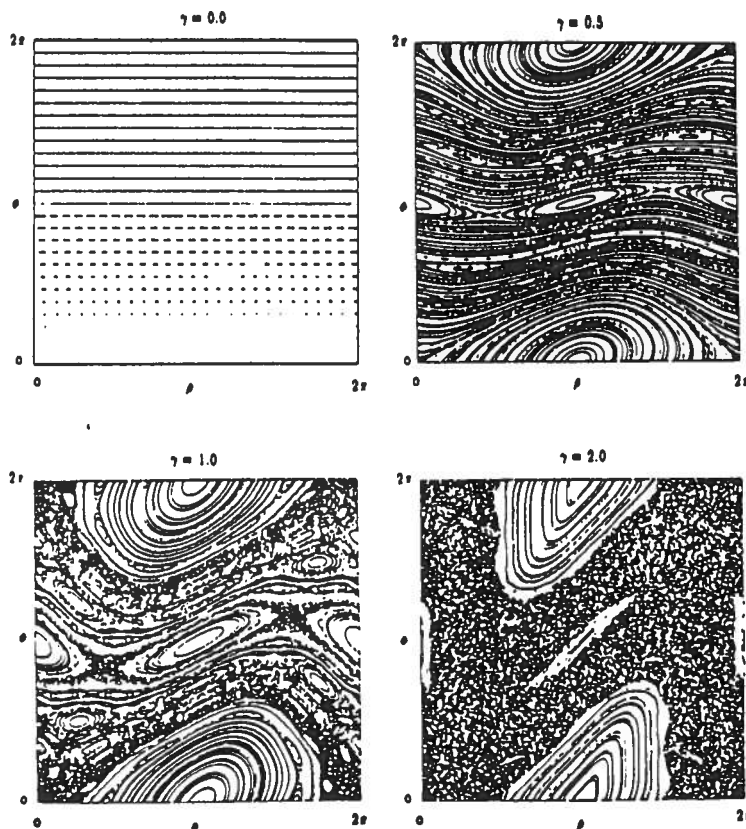


Figure 5. Iterates of the standard map (17) for 729 different initial conditions, ρ_0, ϕ_0 . The mapping is iterated 300 times for each initial condition.

$$V(z) = \frac{c(z) - c_0}{c_0} = -gz \quad (14)$$

with z positive down. The bottom slope $z'_b(r)$ is easily computed from (13). The range increment $B(\theta)$ can be computed using (14) and the ray equations (1),

$$B(\theta) = \frac{2}{g} \tan \theta \approx \frac{2}{g} \theta. \quad (15)$$

Inserting these expressions for the bottom slope and range increment into the mapping (12) gives

$$\theta_{n+1} = \theta_n + 2kh \sin kr_n, \quad (16a)$$

and

$$r_{n+1} = r_n + \frac{2}{g} \theta_{n+1}. \quad (16b)$$

In terms of the dimensionless variables $\rho_n = kr_n$ and $\phi_n = 2k\theta_n/g$ these equations become

$$\phi_{n+1} = \phi_n + \gamma \sin \rho_n, \quad (17a)$$

and

$$\rho_{n+1} = \rho_n + \phi_{n+1}, \quad (17b)$$

where the stochasticity parameter

$$\gamma = \frac{4k^2h}{g}. \quad (18)$$

The dimensionless mapping (17) has been extensively studied by others (see, e.g., Lichtenberg and Lieberman, 1982). It is referred to as the "standard map." The mapping depends on the single dimensionless parameter γ which, in our case, is four times the ratio of bottom curvature to ray curvature. It is easily verified that the mapping is area-preserving,

$$\det \begin{bmatrix} \frac{\partial \phi_{n+1}}{\partial \phi_n} & \frac{\partial \phi_{n+1}}{\partial \rho_n} \\ \frac{\partial \rho_{n+1}}{\partial \phi_n} & \frac{\partial \rho_{n+1}}{\partial \rho_n} \end{bmatrix} = 1. \quad (19)$$

This condition, which may be thought of as a discrete form of Liouville's theorem, guarantees that the Hamiltonian character of the ray equations (1) is faithfully reproduced in the mapping (17). Stated somewhat differently, area-preservation (19) dictates that ϕ_n and ρ_n are canonically conjugate variables (like z and p in the ray equations (1)).

The simplest way to study the mapping is to compute its iterates for a set of initial conditions (ϕ_0, ρ_0) . Some examples are shown in figure 5. Note that ϕ_n and ρ_n are plotted modulo 2π . This is because the mapping (17) is 2π periodic in both variables. Results for several values of stochasticity parameter γ are given. If $\lambda = 2\pi/k = 100$ m and $g = 0.067$ km⁻¹ then $\gamma = 0, 0.5, 1.0, \text{ and } 2.0$ correspond to $h = 0, 2.1, 4.2$ and 8.4

(14)

easily computed from
using (14) and the ray

(15)

d range increment into

(16a)

(16b)

and $\phi_n = 2k\theta_n/g$ these

(17a)

(17b)

(18)

extensively studied by
(19). It is referred to as
the single dimensionless
ratio of bottom curvature
mapping is area-preserving,

(19)

discrete form of Liouville's
theorem of the ray equations (1)
stated somewhat differently,
are canonically conjugate

to compute its iterates for
values are shown in figure 5.
This is because the mapping
exists for several values of
 $r = 100$ m and $g = 0.067$
with $h = 0, 2.1, 4.2$ and 8.4

mm, respectively. This figure should be interpreted in precisely the same way that figure 1 was interpreted. When, for a given ray, successive iterates lie on smooth curves, the motion is regular. A succession of iterates that fills an area in an apparently random way signifies chaotic motion. This figure shows the same qualitative behavior that was seen in figure 1. The stochasticity parameter γ , like δ in figure 1, is a measure of the strength of a nonintegrable (range-dependent) perturbation to an integrable (range-independent) problem. As γ is increased chaotic seas surrounding regular islands are formed. A further increase in γ causes neighboring chaotic seas to merge. For values of γ less than the critical value $\gamma_c \approx 0.97$, the chaotic seas are all bounded. For $\gamma > \gamma_c$ a large chaotic sea exists wherein ray trajectories may wander without bound in the $\phi - \rho$ plane. This phenomenon is referred to as "global chaos".

3.2 Lyapunov Exponents

Lyapunov exponents for the mapping (17) (in base 2 these have units bits per bounce) are computed in much the same way that they were computed for the continuous ray trajectories. Differentiating the mapping (17) gives

$$\begin{bmatrix} d\phi_{n+1} \\ d\rho_{n+1} \end{bmatrix} = M_{n+1} \begin{bmatrix} d\phi_n \\ d\rho_n \end{bmatrix} \quad (20)$$

where, by area-preservation, the determinant of the real 2×2 matrix M_{n+1} is 1. Iterating (20) gives

$$\begin{bmatrix} d\phi_n \\ d\rho_n \end{bmatrix} = J_n \begin{bmatrix} d\phi_0 \\ d\rho_0 \end{bmatrix} \quad (21)$$

where the Jacobi matrix $J_n = M_n M_{n-1} \dots M_1$ also has determinant 1.

Like equation (9) this equation can be used to study sensitivity to initial conditions. The same argument leading to our earlier definition of the Lyapunov exponent (11) applies here. The Lyapunov exponent for the mapping (17) is then

$$\nu \equiv \lim_{n \rightarrow \infty} \frac{1}{n} \ln |\lambda_n^{(1)}| \quad (22)$$

where $|\lambda_n^{(1)}|$ is the modulus of the larger of the two eigenvalues of J_n . We defer until later giving an example of such a calculation.

3.3 Eigenrays

We turn our attention now to eigenrays. Because our analysis is based on the mapping (17) we restrict our attention to situations in which both source and receiver lie on the bottom. Specifically, we examine the behavior of eigenrays as the range r between source and receiver increases. Fans of rays for both a flat bottom and a sinusoidal bottom with amplitude $h = 10$ cm and wavelength $2\pi/k = 200$ m are shown in figure

6. In both cases the sound speed gradient $c_0 g = 0.1 \text{ sec}^{-1}$. These correspond to stochasticity parameters of $\gamma = 0$ and $\gamma = 5.9$, respectively. These models are used to produce all of the numerical results shown in this section. For $\gamma = 5.9$ almost all rays are chaotic.

Eigenrays for the mapping are easily found by constructing the curves $r_n(\theta_0)$, range vs. launch angle for rays which have $n - 1$ bottom bounces. Several examples of such curves are shown in figure 7. Eigenrays for a receiver at range r correspond to the solutions of $r_n(\theta_0) = r$, i.e., intersections of a curve $r_n(\theta_0)$ with a horizontal line. Of course, to find all of the eigenrays at range r this process must be repeated for many values of n . Before we show the results of carrying out this procedure, however, it is instructive to take a closer look at one of the $r_n(\theta_0)$ curves for the sinusoidal bottom.

Figure 8 shows a succession of blow ups of the $r_{13}(\theta_0)$ curve for $5.0^\circ < \theta_0 < 5.5^\circ$. In the uppermost curve the sampling interval $\Delta\theta = 10^{-4}$ degrees. In the lowermost curve $\Delta\theta = 10^{-8}$ degrees. It would have been difficult to guess that such a small sampling interval is necessary after only 12 bounces. This number is not absolute. Our numerical simulations indicate that for each additional two bounces $\Delta\theta$ must be decreased by roughly a factor of ten.

Figure 9 shows the number of eigenrays N as a function of range r , computed using the procedure outlined above. Because of the huge difference in the number of eigenrays for the flat and sinusoidal bottom cases, different angular apertures were used: 4° for the flat bottom and 0.5 degrees for the sinusoidal bottom. This figure shows clearly that for the flat bottom $N(r)$ grows linearly while for the sinusoidal bottom $N(r)$ grows exponentially ($\sim \exp(r/1.9 \text{ km})$ in this figure).

Because the number of eigenrays is growing exponentially in the sinusoidal bottom case, energy conservation dictates that the corresponding average intensity

$$I_{av} = \frac{1}{N} \sum_{i=1}^N \left| \left[\frac{\partial r}{\partial \theta_0} \right]_i \theta_i \right|^{-1}, \quad (23)$$

where θ_i is the launch angle of an eigenray, should decay exponentially in range. This quantity is plotted as a function of range in figure 10. In this figure $I_{av} \sim \exp(-r/2.0 \text{ km})$. This is consistent with exponential growth of the number of eigenrays.

One would expect that the exponential growth of the number of eigenrays and the corresponding exponential decay of their average intensities is related to an average Lyapunov exponent for the rays under consideration (recall $5.0^\circ < \theta_0 < 5.5^\circ$). Because these rays are predominantly chaotic and most lie in the same chaotic sea the notion of an "average Lyapunov exponent" is a sensible one. For an individual ray

0.1 sec⁻¹. These = 5.9, respectively. Results shown in this

structuring the curves 1 bottom bounces.

Eigenrays for a $r_n(\theta_0) = r$, i.e., Of course, to find repeated for many out this procedure, of the $r_n(\theta_0)$ curves

$r_3(\theta_0)$ curve for 5.0° interval $\Delta\theta = 10^{-4}$

It would have been necessary after only numerical simulations must be decreased by

function of range r, because of the huge and sinusoidal bottom

flat bottom and 0.5 clearly that for the flat bottom $N(r)$ grows

exponentially in the at the corresponding

(23)

decay exponentially in range in figure 10. In agreement with exponential

of the number of rays of their average for the rays under use these rays are in the sea the notion of for an individual ray

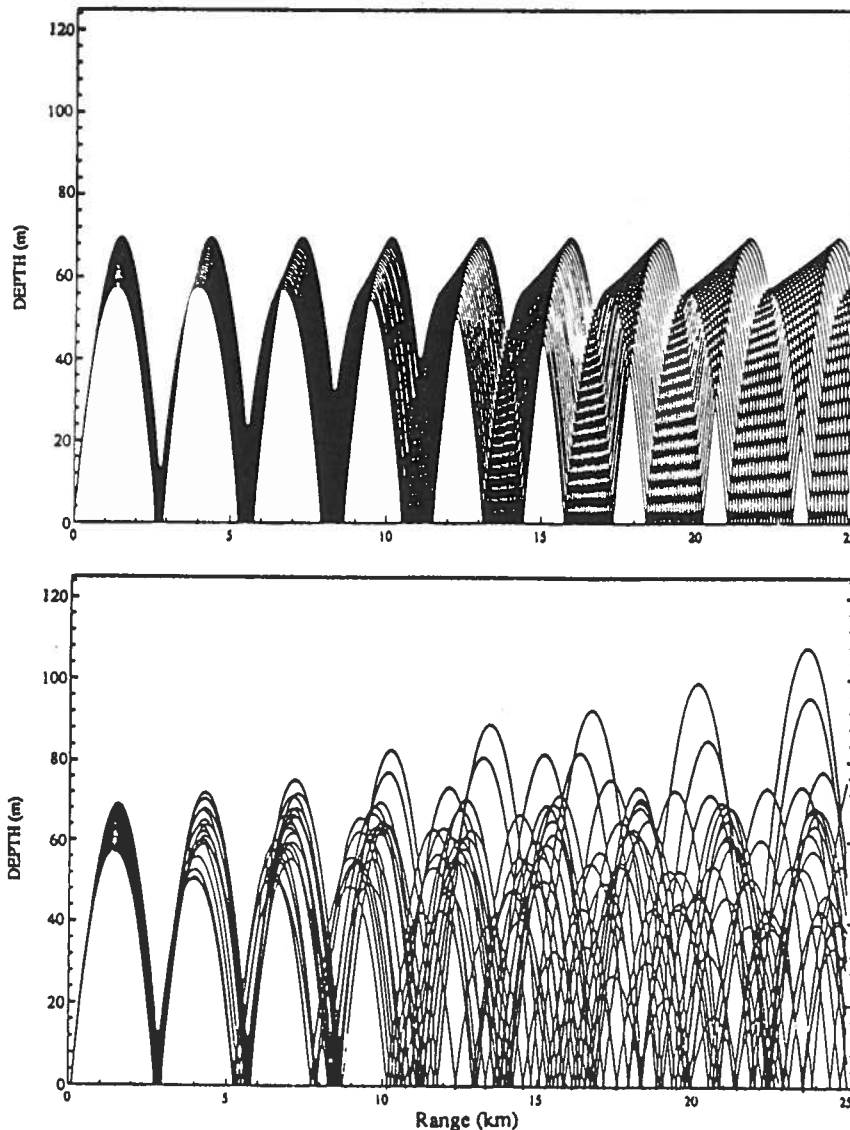


Figure 6. Fans of rays corresponding to launch angles $5.0^\circ < \theta_0 < 5.5^\circ$ over flat (upper panel) and sinusoidal (lower panel) bottoms.

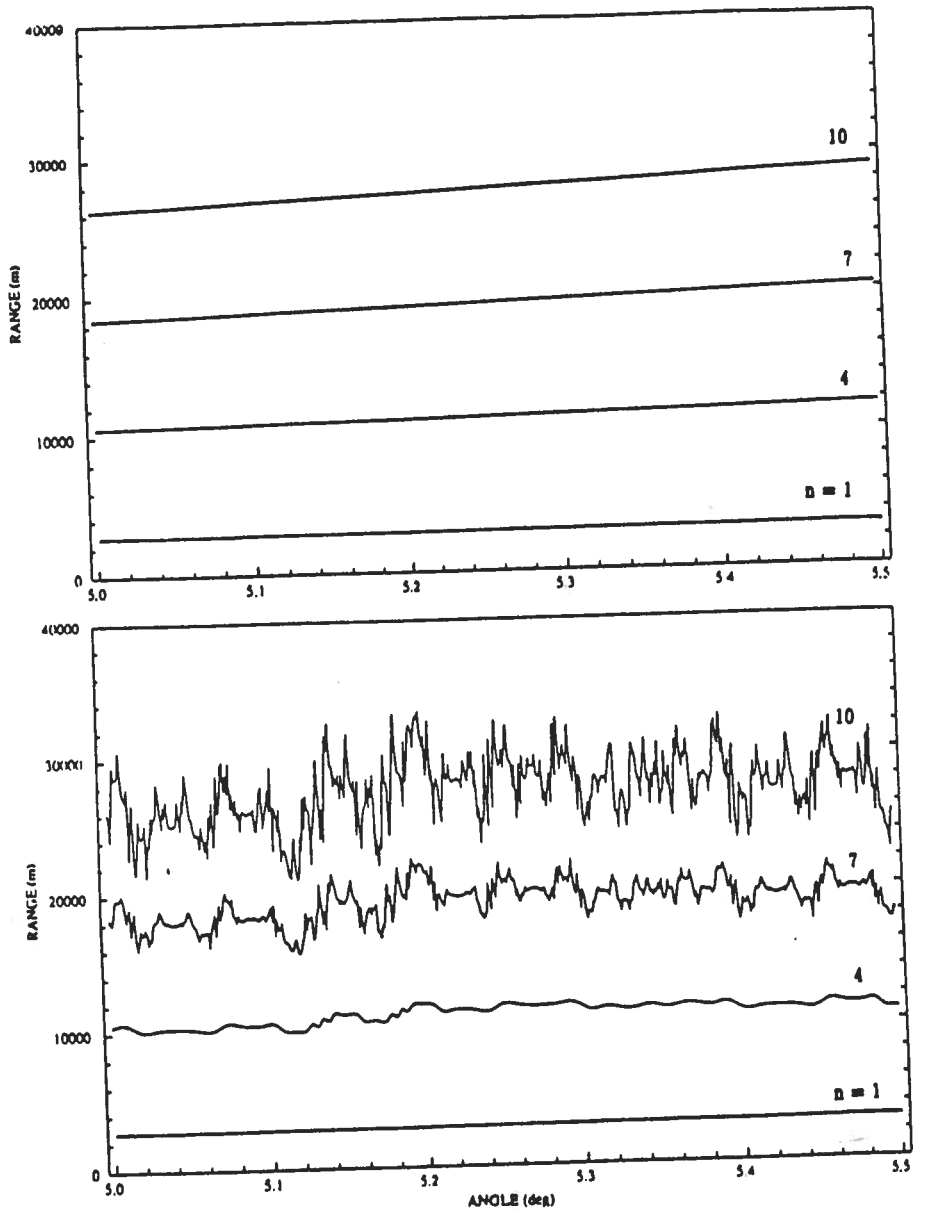


Figure 7. Plots of r_n vs. θ_0 for flat (upper panel) and sinusoidal (lower panel) bottoms.

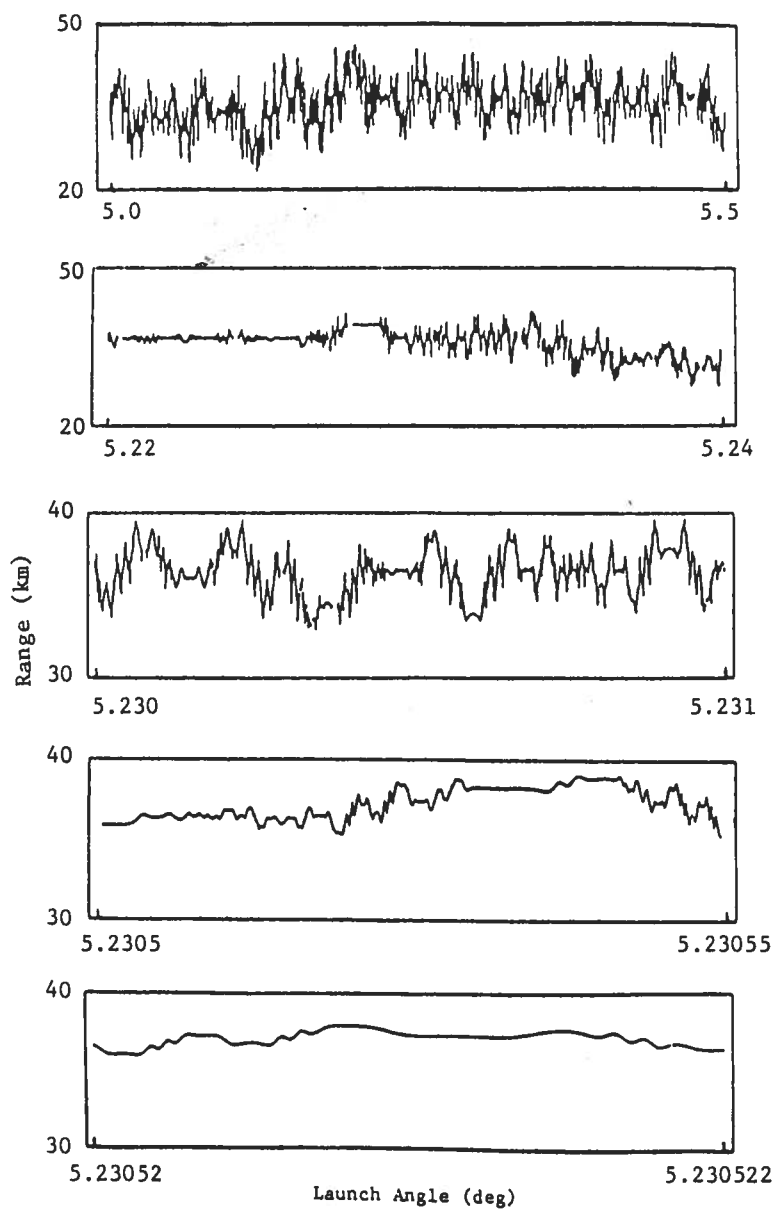
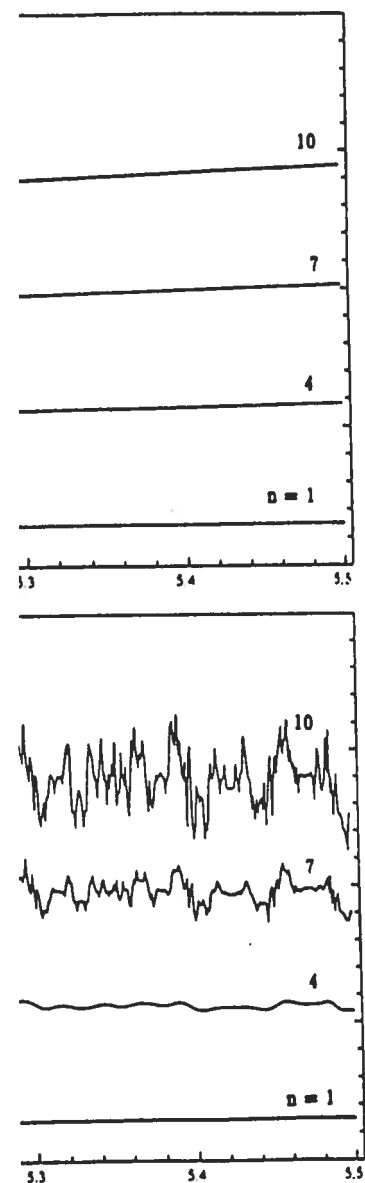


Figure 8. Plots of r_{13} vs θ_0 for a sinusoidal bottom. Each plot is a magnified version of some portion of the plot above.

and sinusoidal (lower panel) bottoms.

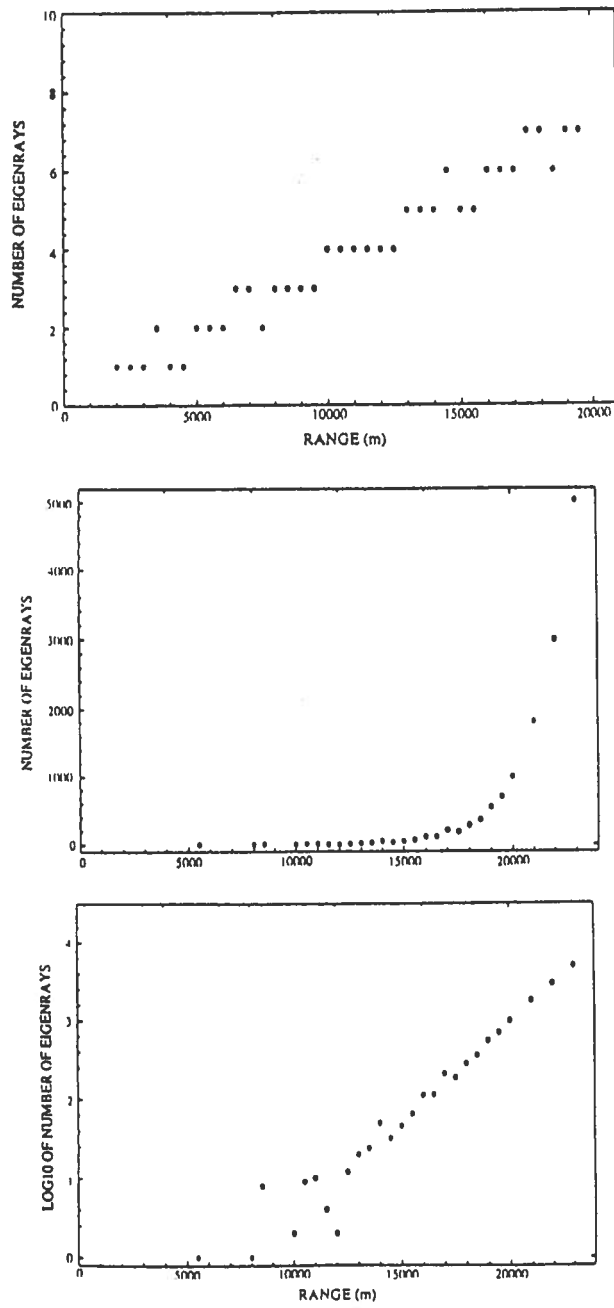


Figure 9. Plots of the number of eigenrays N as a function of range r . Upper panel: N vs r for a flat bottom. Center panel: N vs r for a sinusoidal bottom. Lower panel: $\log N$ vs r for a sinusoidal bottom.

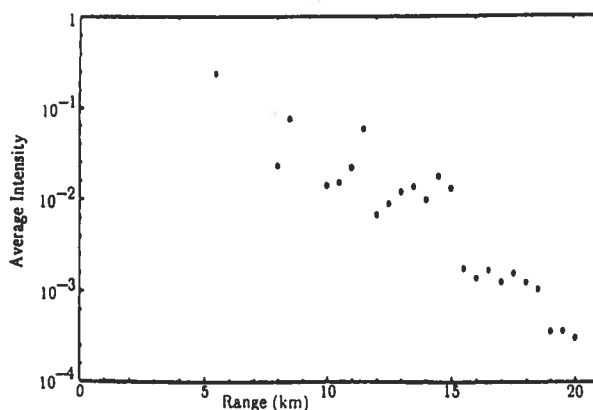


Figure 10. Plot of average eigenray intensity as a function of range for the sinusoidal bottom problem.

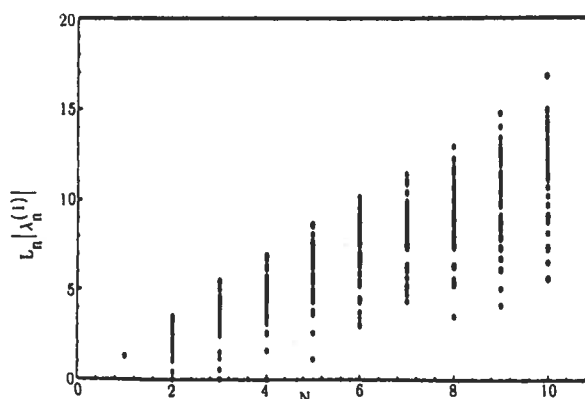


Figure 11. Plot of $\ln |\lambda_n^{(1)}|$ vs. n for 51 rays whose launch angle $5.0^\circ \leq \theta_0 \leq 5.5^\circ$. The average slope of the plotted points is an estimate of the average Lyapunov exponent.

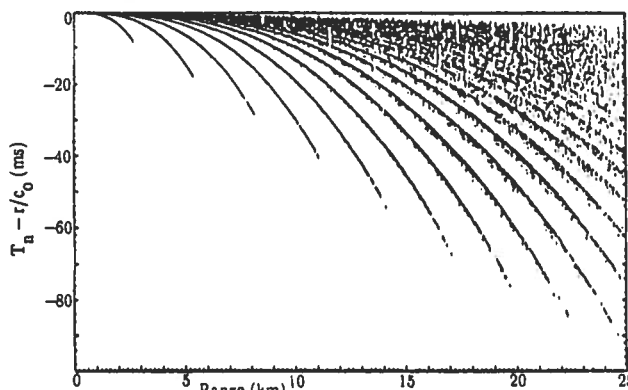
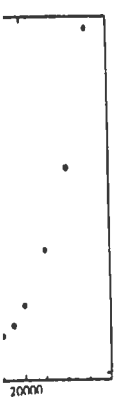


Figure 12. Plot of reduced travel time $T_N - r/c_0$ vs. range r for the sinusoidal bottom problem. Each cluster of points correspond to a fixed number of bottom bounces N , with N increasing upwards and to the right.



of range r . Upper panel: N vs r
 plot. Lower panel: $\log N$

the Lyapunov exponent ν is defined by equation (22). To maintain consistency with the results shown in figures 6-10, however, we have plotted in figure 11 $\ln |\lambda_n^{(1)}|$ vs n , $n = 0, 1, 2, \dots, 10$, for 51 rays in the band $5.0^\circ < \theta_0 < 5.5^\circ$. The average slope of the points plotted is an estimate of the average Lyapunov exponent ν_{av} . From the figure $\nu_{av} \approx 1.3/\text{bounce}$. Using 2.9 km/bounce as an average range increment - see figure 6 or 7 - this corresponds to $\nu_{av} \approx (2.2 \text{ km})^{-1}$. This is in rough agreement with our earlier results.

The distribution of travel times T as a function of range r gives additional insight into the complexity of the wavefield under chaotic conditions. In figure 12, $T(r)$ is plotted for many (not all) rays in the band $1.0^\circ < \theta_0 < 5.0^\circ$. Each cluster of points in this figure corresponds to a different number of bottom bounces n . This figure shows that travel times for rays which have hit the bottom only a few times are tightly bound and clusters corresponding to different n are distinct. As n increases, travel time spreads grow and clusters corresponding to different n overlap with their neighbors. This figure shows that after a small number of bounces the wavefield is highly structured and predictable. After a large number of bounces, however, the wavefield is largely unstructured and appears to be unpredictable. This is chaos.

4. A SEARCH FOR WAVE CHAOS

Our discussion up until now has focused on chaotic behavior of ray trajectories in models of range-dependent oceanic waveguides. It is natural to ask, "To what extent does the unpredictability associated with chaotic ray trajectories carry over to finite frequency wavefields?" In this section we present some preliminary numerical results which address this question. It is natural to refer to chaotic behavior in finite frequency wavefields, if it exists, as "wave chaos."

In another context this phenomenon, a controversial one, is referred to as "quantum chaos." To date, most of the work on quantum chaos (see, e.g., Berry, 1987) has been concerned with the distribution of energy levels of quantum systems which exhibit chaotic motion in the classical limit. It is known that these energy levels obey different statistics in (a) systems which are classically chaotic and (b) systems which are classically regular. These important results provide little insight into our underwater acoustics problem, however. The reason is that these results apply to the solutions to boundary value problems whereas our underwater acoustic waveguide problems are initial value problems.

In this section, we confine our attention to one of many ideas which might be used to investigate wave chaos. The idea is reversibility or, more specifically, lack of reversibility in chaotic systems. The ray equations (1) can be integrated backwards in range by simply changing the sign of r . It is straightforward to verify that under regular conditions a ray trajectory can be computed forward, out to a very long range, and backwards, only

to recover the initial conditions, $z(0)$, $p(0)$. For a chaotic trajectory this procedure does not work at ranges longer than a few e-folding distances, ν^{-1} . The reason is that at longer ranges the initial conditions of the ray will have been forgotten. One way to investigate wave chaos is to ask whether finite frequency wavefields "forget" their initial conditions in a similar fashion.

We have addressed this question by examining solutions to the parabolic wave equation,

$$i \frac{\partial \psi}{\partial r} + \frac{1}{2k_0} \frac{\partial^2 \psi}{\partial z^2} - k_0 V(z,r) \psi = 0, \quad (24)$$

which are computed using the split-step Fourier algorithm (Tappert, 1977). In (24), $k_0 = \omega/c_0$ where ω is the angular frequency of the sound waves and the acoustic pressure

$$u(z,r) = \psi(z,r) (k_0 r)^{-1/2} e^{ik_0 r}. \quad (25)$$

It should be noted that the wave equation (24) reduces to the ray equations (1) in the high frequency limit. The split step Fourier algorithm is well suited to looking at reversibility because depth dependent complex wavefields $\psi(z)$ can be stepped backwards as well as forwards in range using this technique.

Figure 13 shows examples of forward and back propagated fields out to a range of $r_{\max} = 18.53$ km. These wavefields were computed using an acoustic frequency of 16 kHz. The azimuthal spreading factor in (25) was neglected in both the forward and back propagation problems. The initial ($r = 0$) field for the forward propagation calculation was a narrow downward directed gaussian beam. The ocean structure was chosen to coincide with the sinusoidal bottom problem described in the previous sections. The potential $V(z,r)$ is given by (14) with $c_0 = 1510$ m s⁻¹ and the bathymetry is given by (13) with $h = 61$ cm and $2\pi/k = 185$ m. This choice of parameters corresponds to a stochasticity parameter (eq. 17) $\gamma = 44.8$. The PE runs require a finite ocean depth and bottom sound speed. We used 98 m and 1740 m s⁻¹, respectively. In the back propagation calculation, the complex conjugate of the forward propagated field at r_{\max} is used as the initial condition and the bathymetry is reversed.

In this environment ray trajectories are highly chaotic and one would expect that ray theory accurately describes the acoustic wavefield at 16 kHz. Figure 13 shows rather dramatically, however, that the wavefield at $r = r_{\max}$ has not forgotten its initial conditions. Furthermore, our investigation of the dependence of back-propagated fields on r_{\max} indicates that the results degrade slowly as r_{\max} is increased. There is no evidence of exponential degradation of back-propagated fields. These and other numerical simulations that we have performed suggest that wave chaos does not exist.

To maintain
however, we have
r 51 rays in the
nts plotted is an
the figure $\nu_{av} \approx$
increment - see
This is in rough

of range r gives
ld under chaotic
all) rays in the
figure corresponds
shows that travel
times are tightly
distinct. As n
ing to different n
r a small number
le. After a large
unstructured and

behavior of ray
les. It is natural
ated with chaotic
" In this section
ress this question.
y wavefields, if it

one, is referred to
antum chaos (see,
n of energy levels
classical limit. It
cs in (a) systems
classically regular.
derwater acoustics
y to the solutions
oustic waveguide

many ideas which
ersibility or, more
ray equations (1)
the sign of r. It
; a ray trajectory
d backwards, only

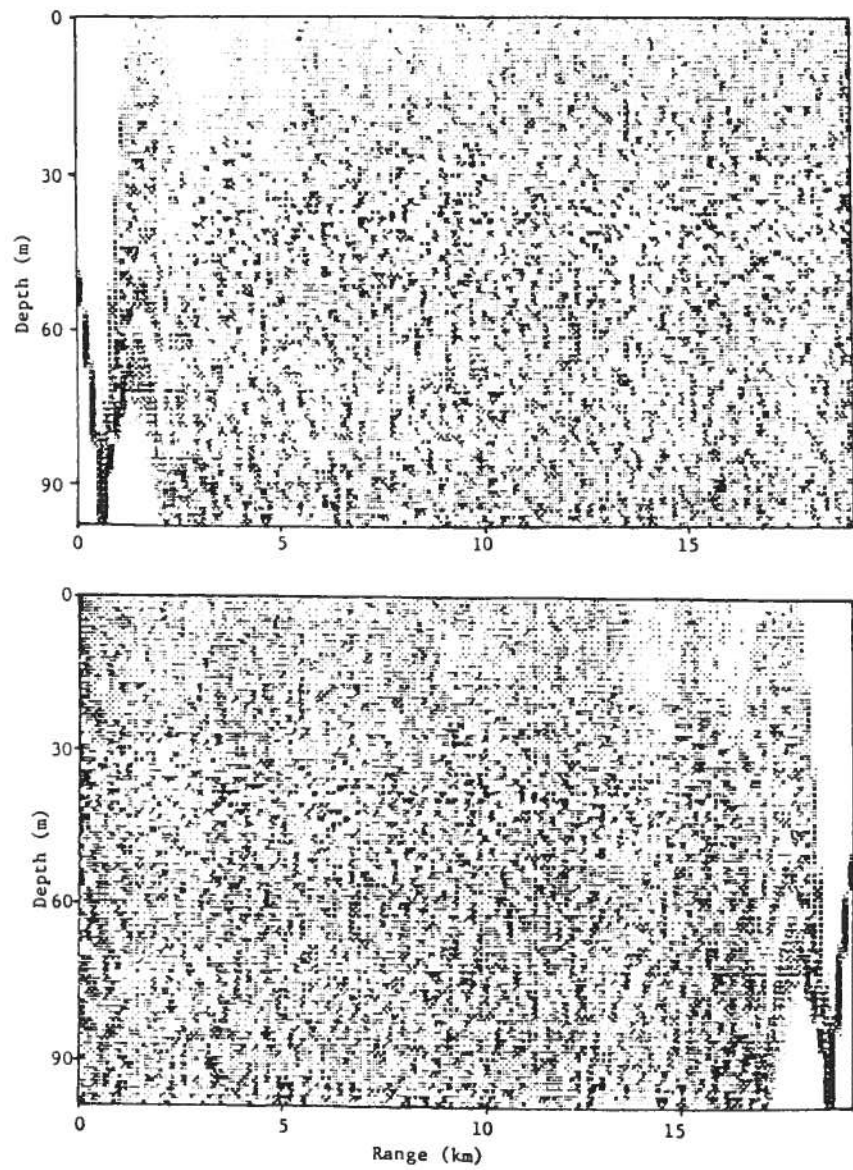


Figure 13. Gray scale plots of the logarithm of the intensity of forward (upper panel) and back (lower panel) propagated acoustic wavefields. The ocean model is described in the text.

5. DISCUSSION AND SUMMARY

We have argued that the generic range-dependent sound propagation problem differs in a fundamental way from the range-independent problem, at least in the geometric limit. In the range-dependent problem at least some ray trajectories exhibit chaotic motion wherein neighboring trajectories diverge from each other exponentially. Under conditions in which ray trajectories are predominantly chaotic we have shown that the complexity of the geometric wavefield grows exponentially in range. In the range independent problem, wavefield complexity also grows in range but at a much slower (power law) rate.

In this paper we have restricted our attention to periodically range-dependent models of ocean sound channels. It is natural to ask how this situation differs from the more realistic nonperiodic range-dependent problem. An important difference is that in the latter problem the phase space (z,p,r) is not bounded. As a result Poincare sections cannot be constructed. Power spectra and Lyapunov exponents are still useful diagnostic tools to identify chaotic motion. In all cases there is uncertainty associated with taking the limit $r \rightarrow \infty$ in estimating the Lyapunov exponent (11). The best one can do is to say that over some range of r ν appears to be approaching a well defined value. We are currently investigating the behavior of ray trajectories in numerically simulated ocean sound channels containing realistic mesoscale induced perturbations. The results are not yet complete.

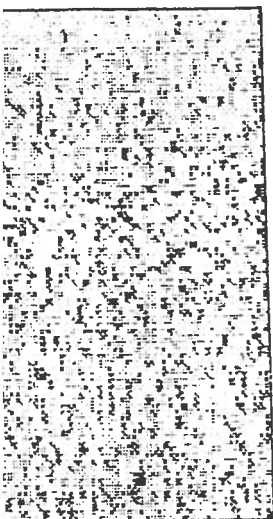
Under chaotic conditions ray trajectories are not computable, due to extreme sensitivity to initial conditions, beyond some finite predictability horizon. This leads us to question whether there might be a fundamental limitation on our ability to compute finite frequency wavefields. The preliminary numerical experiments which we have performed suggest that no such limitation exists.

ACKNOWLEDGEMENTS

This work was supported by the Office of Naval Research and the National Science Foundation.

REFERENCES

- Abdullaev, S.S., and G.M. Zaslavskii (1988) "Fractals and Ray Dynamics in a Longitudinally Inhomogeneous Medium," *Sov. Phys. Acoust.* **34**(4), 334-336.
- Berry, M.V. (1987) "Quantum Chaology," *Proc. Roy. Soc. Lon. A* **413**, 183-198.
- Henon, M. (1983) "Numerical Exploration of Hamiltonian Systems," in Chaotic Behavior of Deterministic Systems (Les Houches Lectures 36), edited by G. Iooss, R.G.H. Helleman, and R. Stora, North Holland, Amsterdam, 171-271.



15



15

ty of forward (upper panel) and
model is described in the text.

Lichtenberg, A.J., and M.A. Lieberman (1982) Regular and Stochastic Motion, Springer Verlag, New York, 499 pp.

Munk, W.H. (1974) "Sound Channel in an Exponentially Stratified Ocean with Application to SOFAR," J. Acoust. Soc. Am. 55, 220-226.

Palmer, D.R., M.G. Brown, F.D. Tappert, and H.F. Bezdek (1988) "Classical Chaos in Nonseparable Wave Propagation Problems," Geophys. Res. Lett. 15(6), 569-572.

Tappert, F.D. (1977) "The Parabolic Approximation Method, in Lecture Notes in Physics, vol. 70, Wave Propagation and Underwater Acoustics, J.B. Keller and J.S. Papadakis (eds), Springer Verlag, New York, 224-287.